ELSEVIER

Materials Science and Engineering A 485 (2008) 422–427

MATERIALS SCIENCE & ENGINEERING A

www.elsevier.com/locate/msea

Silicon nitride compressive creep behavior in argon atmosphere

Cosme Roberto Moreira da Silva [a,*], Flaminio Levy Neto [a], José Alexander Araújo [a], Claudinei dos Santos [b]

[a] *Universidade de Brasília, UNB, Brasília-DF 70910-900, Brazil*

[b] *Faculdade de Engenharia Química de Lorena, DEMAR, Lorena 12600-000, Brazil*

Received 10 February 2007; received in revised form 1 August 2007; accepted 30 August 2007

Abstract

Gas pressure sintering, using pure neodymium oxide and a mixture of neodymium oxide and yttrium oxide as sintering aids, was used to process silicon nitride samples. The short-term compressive creep behavior in argon was evaluated over a stress range of 50–300 MPa, and temperature range of 1250–1400 °C. Microstructural analysis by X-ray diffractometry and transmission electron microscopy showed that secondary crystalline phases, which form from the remnant glass, are dependent upon composition and percentage of additives. Stress exponent values near to unity were obtained for lower stress and temperature testing and materials with low glass content, suggesting grain boundary diffusion accommodation processes. Cavitation will thereby become prevalent with increase in stress, temperature and amount of the grain boundary phase, and decrease in the degree of crystallization of the intergranular phase.

Keywords: Silicon nitride; Creep; Ceramics

1. Introduction

Silicon nitride is considered as a strong candidate for fabrication of high efficiency turbine components, considering its low thermal expansion and high thermal-shock resistance [1]. Its thermal expansion coefficient is around $2.9 \times 10^{-6} < \alpha < 3.6 \times 10^{-6}\,K^{-1}$ for $20 < T < 1500\,^{\circ}C$ [1,3]. In each of its structural modifications, α and β, silicon nitride has a unique combination of properties. It is strong, hard, wear resistant and stable to higher than 1800 °C [2]. The use of silicon nitride in turbine components would lead to weight savings and an increase in their operating temperatures, which would in turn increase fuel efficiency. The covalent character of the Si–N bonds and the extremely low self-diffusion coefficients of silicon and nitrogen increase the difficulty to sinter Si_3N_4. Sintering aids must be added to promote liquid phase sintering in such a way to achieve appropriate densification. During sintering, additives will react with silicon nitride and native SiO_2 on Si_3N_4 particles surfaces. The subsequent formation of the liquid oxinitride phase promotes particle rearrangement, α-Si_3N_4 solution and subsequent β-Si_3N_4 reprecipitation, leading to densification. The intergranular phase formation is strongly important to the final high temperature properties [4]. Good densification has been achieved using yttrium oxide as sintering aid [5–8].

Lanthanide oxides are also strong candidate additives, taking into account their relatively high melting points, providing therefore highly refractory remnant amorphous grain boundary phase after sintering. The formed liquid intergranular phase originated from rare-earth sintering aids have high nitrogen content, high viscosity and glass transition temperature, which can improve substantially high temperature mechanical properties [10].

Creep deformation occurs at high temperature when the amorphous grain boundary phase softens, thus permitting relative motion of the grains. Improvement of the refractoriness and reduction of the amount of the sintering aids have dramatically improved the creep resistance of silicon nitride [9]. The approach to improve its mechanical properties at elevated temperature by crystallization of grain boundary phases has also been demonstrated by several researchers [10–12].

Creep of silicon nitride based ceramics has been extensively tested in tension and bending [13–17]. A comprehensive review on Creep Mechanism in Multiphase Ceramic Materials

* Corresponding author.
E-mail address: cosmeroberto@gmail.com (C.R.M. da Silva).

0921-5093/$ – see front matter © 2007 Elsevier B.V. All rights reserved.
doi:10.1016/j.msea.2007.08.080

[18] shows that only few researchers performed tests in those materials under compressive stress. Test atmospheres in these cases were basically air [8,19–22].

The aim of the present investigation is to evaluate short-term compressive creep behavior of gas-pressure sintered silicon nitride with neodymium/yttrium oxides mixtures as sintering aids. Creep tests were performed in argon, in temperature range of 1250–1400 °C and stress range of 50–300 MPa. High temperature creep mechanisms and stress exponent values are correlated to microstructural features observed by TEM and its relationship with the amount and composition of sintering aids and degree of crystallization of grain boundary phase.

2. Experimental procedures

Commercial silicon nitride powder (SNE-10, UBE, Japan) was used for sample fabrication. Yttrium oxide (H.C. Stark, fine grade) and neodymium oxide (99.99%, purity, Johnson Matthey Co., U.K.) were utilized as densification aids. The following steps were used for Y_2O_3/Nd_2O_3 powder mixture fabrication: The two powders (1:1 mol) were at first mixed in polypropylene containers during 24 h, using dry ethanol as dispersing agent. The obtained fluid was dried, milled and heated up to 1000 °C, remaining at this temperature for 3 h. The resulting product was milled during 24 h, to obtain the adequate particle size distribution, for the sintering step.

Wet milling of silicon nitride and sintering aids during 48 h in dry ethanol was used to produce samples of two different compositions (% in weight):

Composition A: 92% Si_3N_4 + 8% neodymium oxide.
Composition B: 92% Si_3N_4 + 8% yttrium/neodymium oxides mixture.

The samples were uniaxial and isostatically cold pressed at 300 MPa, as cylinders with approximately 2.5 mm diameter and 5.0 mm high after sintering. Discs with 20.0 mm diameter and 3.0 mm high were also cold pressed and sintered under the same conditions to allow X-ray diffractometry analysis. The gas pressure sintering was performed at 1800 °C and 4 MPa of maximum gas pressure. The materials A and B reached densities above 99% of theoretical. X-ray diffractometry analysis was performed in each composition, using a Philips PW 1840 diffractometer with Cu Kα radiation.

Thin foils for transmission electron microscopy examinations were prepared by mechanical polishing and ion beam thinning. The TEM samples were cut parallel to the applied stress axis of the compressive crept samples. The microscope accelerating voltage was in a range of 120–300 KV.

The furnaces used in the rigs were standard molybdenum-wound furnaces PCA-10, produced by Metals Research Ltd., Cambridge. To monitor specimen temperature and control furnace temperature, 6% Rhodium-Platinum against 30% Rhodium-Platinum thermocouples were used. The compression of the specimen on creep testing was sensed and measured by a LVDT.

Each silicon nitride sample was at first measured and inserted between the two silicon carbide discs, previously positioned between the extremity of the loading bar and the base of the loading molybdenum support tube. The furnace was then lifted to a position where the top end of the connecting port could be clamped and sealed against the lower face of the top plate. A stable argon flux was introduced into the system, with a silicone oil bubble at the gas outlet line, giving necessary backpressure to the system. After these procedures, the chart recorder and the adjustment voltage regulator feeding the LVDT were switched on, the follower pin of the LVDT was positioned against the horizontal bar carried on the plunger and a time of 30 min was allowed before the loads were applied to the system, enabling the various parts of the rig to equilibrate before creep displacements were recorded. Tests stress range were 50–300 MPa and temperature range 1250–1400 °C.

3. Experimental results and discussion

3.1. Particle size distribution

Fig. 1 presents particle size distribution of starting powders and final silicon nitride compositions, before and after wet milling. The obtained results show the effectiveness of wet milling.

Representative micrographs of compositions A and B, before and after creep tests are presented on Figs. 2 and 3. There is no evidence of considerable grain growth or aspect ratio alterations in the crept specimens.

3.2. Crystalline phases of sintered samples.

The identified crystalline phases at composition A after sintering, Fig. 4, were β-Si_3N_4 (H), $Nd_4Si_3O_{12}$ (H), $Nd_2Si_3O_3N_4$ (T) and $Nd_{10}(SiO_4)_6$ (T). For composition B, Fig. 5, such compositions after sintering were basically β-Si_3N_4 (H), $Y_2Si_3O_3N_4$ (T), $Y_2Si_2O_7$ (M) and $Y_{20}N_4Si_{12}O_{18}$ (T). For this composition, neodymium silicates were not detected.

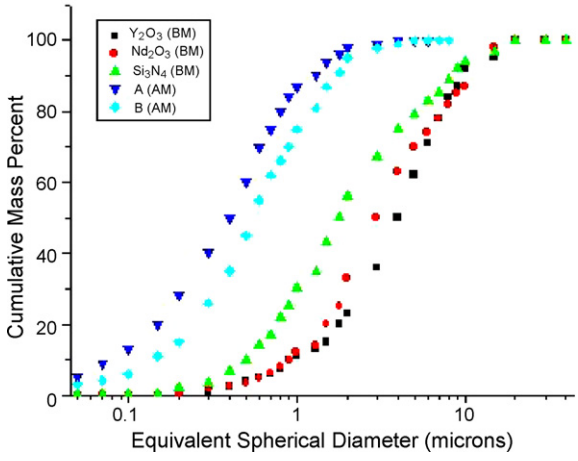

Fig. 1. Particle size distribution of Si_3N_4, Y_2O_3 and Nd_2O_3 powders before wet milling (BM) and compositions A and B after wet milling (AM).

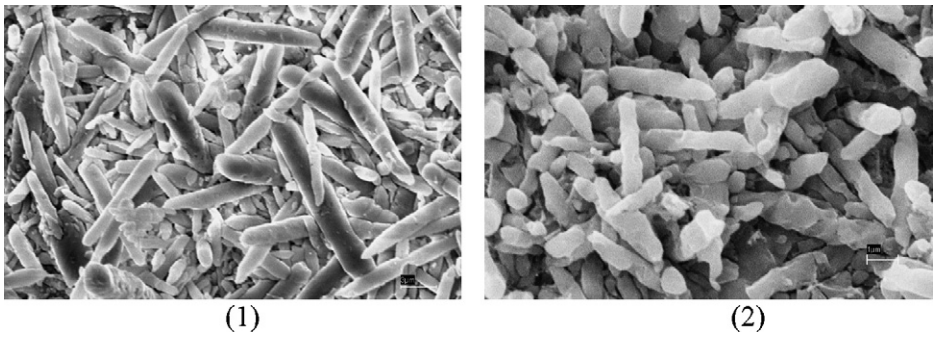

Fig. 2. Representative micrograph of composition A before (1) and after (2) creep tests, at 1350 °C and 300 MPa for 70 h.

Fig. 3. Representative micrograph of composition B before (3) and after (4) creep tests, at 1350 °C and 300 MPa for 70 h.

3.3. Creep results

Figs. 6 and 7 show typical creep curves, for compositions A and B, respectively, tested at 1350 °C and different stress levels. Each creep test was performed during 70 h. Barreling effect was negligible during compression tests. Both compositions exhibit normal creep curves, with a short initial period of decreasing primary creep rate, followed by secondary stage.

Figs. 8 and 9 show creep rate vs. creep strain curves for compositions A and B, tested at 1350 °C, for various stress conditions. All the creep curves obtained show the normal primary creep followed by reasonably defined steady state creep regions.

The stress dependence of the steady state creep rate for compositions A and B are presented in Figs. 10 and 11, respectively.

The obtained stress exponents for composition A were in a range between 0.75 and 1.10, indicative of diffusional creep predominance. Higher stress exponents values were obtained for composition B, within a range from 0.89 to 1.87.The higher stress exponents observed for composition B are attributed to higher amount of amorphous grain boundary phase, which enhances creep deformation by grain boundary sliding and subsequent cavitation. Further MET examinations confirmed that cavitation would prevail, for higher temperature and stresses, in this case.

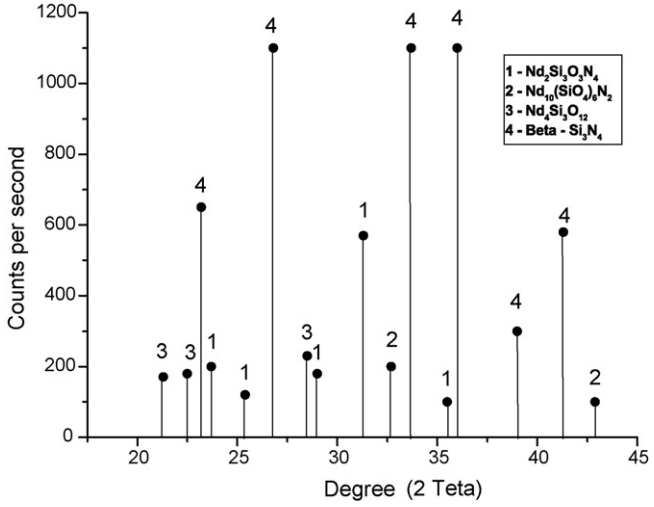

Fig. 4. X-ray diffraction patterns of the sintered composition A.

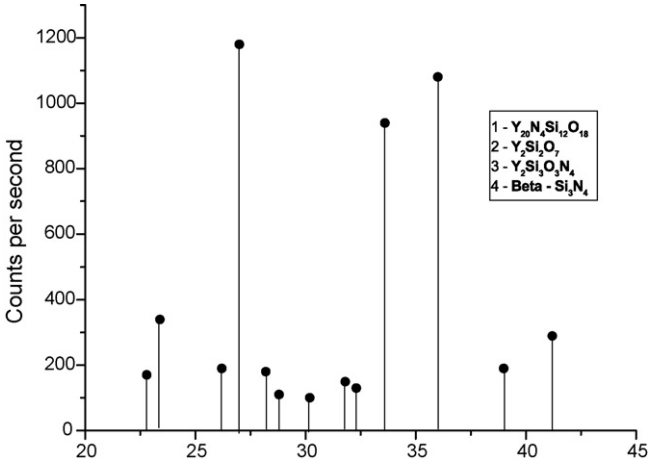

Fig. 5. X-ray diffraction patterns of the sintered composition B.

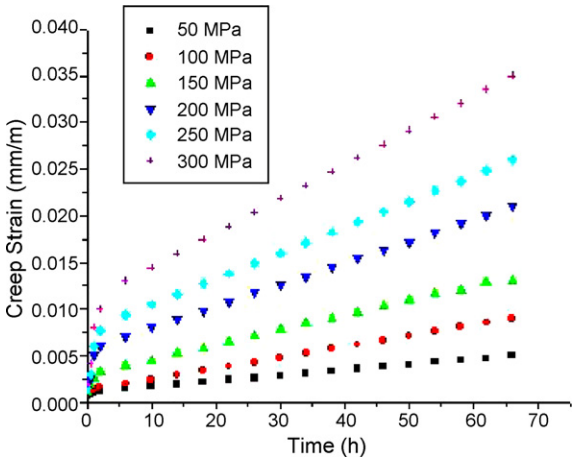

Fig. 6. Typical creep curves, tested at 1350 °C and different stresses, for composition A.

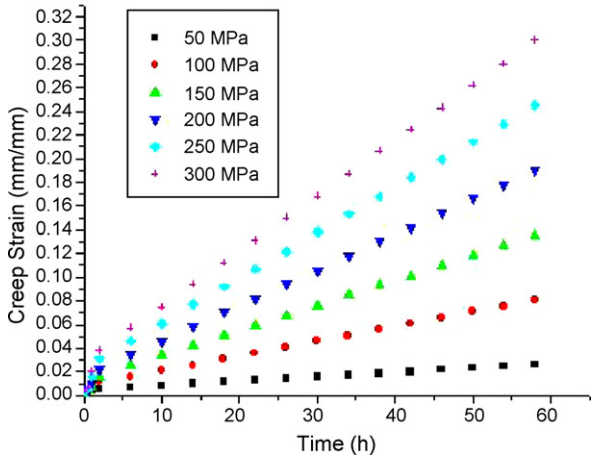

Fig. 7. Typical creep curves, tested at 1350 °C and different stresses, for composition B.

Estimates of creep activation energies were obtained from slopes of graphics at Figs. 10 and 11, giving a range of values between 630 and 660 kJ/mol for composition A and 790 and 810 kJ/mol for composition B.

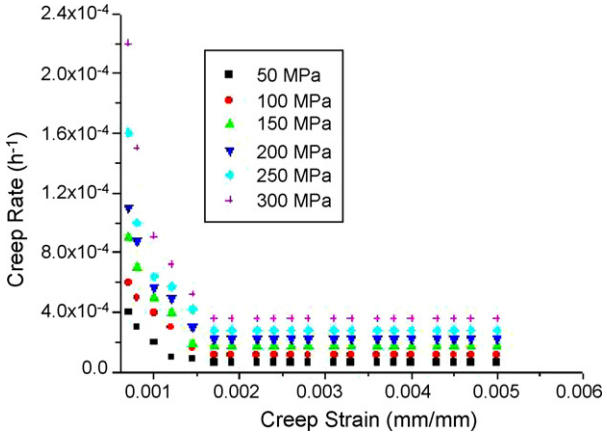

Fig. 8. Creep rate vs. creep strain curves for composition A, tested at 1350 °C under various stress conditions.

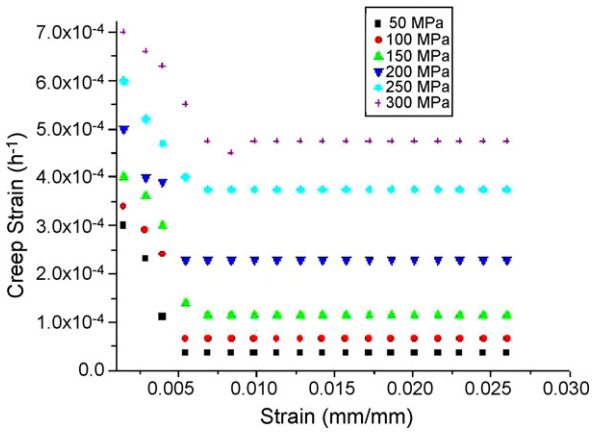

Fig. 9. Creep rate vs. creep strain curves for composition B, tested at 1350 °C under various stress conditions.

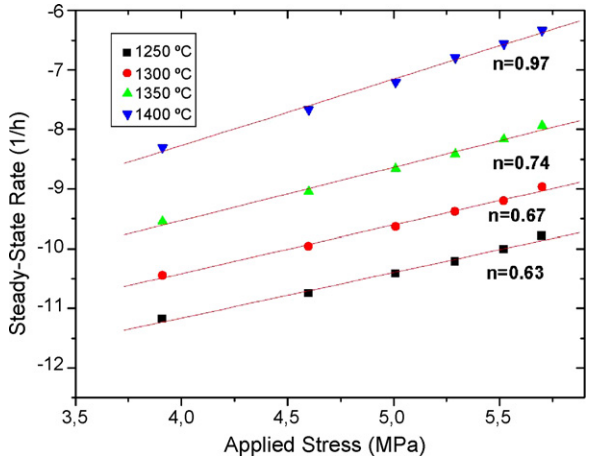

Fig. 10. Stress dependence of steady state creep rates for composition A, under different temperatures.

Activation energies for different kinetic processes in hot pressed silicon nitride, fluxed with MgO, have been reported by Raj and Chyung [27] and Raj and Morgan [23]. In this case, the measured activation energies for creep for viscous grain bound-

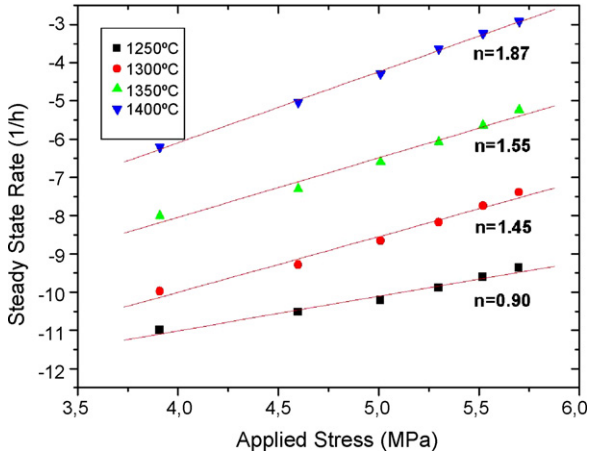

Fig. 11. Stress dependence of steady state creep rates for composition B, under different temperatures.

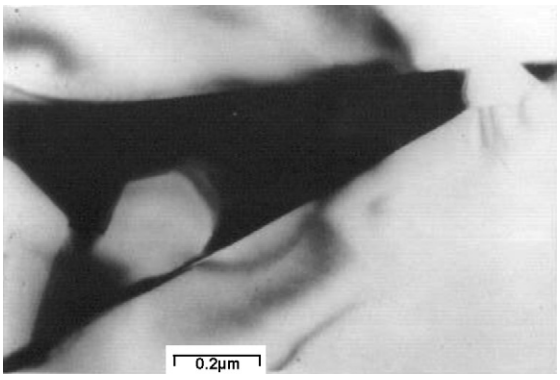

Fig. 12. N-melilite phase (black area) at the hexagonal β-Si_3N_4 grain boundary phase.

ary sliding and diffusional creep were, respectively, 740 and 630 kJ/mol. Assuming that solution-precipitation via medium of the intergranular glassy phase is a phase transformation mechanism, and considering that is difficult to retain Si_3N_4 in a glassy state, it is inferred by Raj and Morgan that activation energy values for creep and viscous grain boundary sliding is related primarily to the high heat of solution of the crystalline phase in the glassy phase [23]. A comprehensive review performed by Cannon and Langdon on creep for Si_3N_4 gives activation energies values near 850 kJ/mol for creep where cavitation prevails, at higher additive content silicon nitride compositions [29].

3.4. Transmission electron microscopy

High resolution transmission electron microscopy has been used before for crept samples examination [1,24,25] in order to reveal the existing fine intergranular and multigrain junction glassy phase of silicon nitride ceramics with additive content. In the present work, energy dispersive microanalysis did not show evidence of neodymium or yttrium solubility in β-Si_3N_4 grains, and all the additions are retained at the silicate phase that involves the hexagonal β-Si_3N_4 (Fig. 12). Amorphous and crystalline phases are retained at grain boundaries and multigrain junctions. A positive identification of the $Nd_2Si_3O_3N_4$ was made by a series of diffraction patterns (Fig. 13). There is no evidence of dislocation activity at the examined samples, either for compositions A or B.

After being cooled under load at the end of creep test, the materials with low amount of glassy phase (A) did not show cavitation. It is considered [26] that existing asperities at grain boundaries were not smoothed out by diffusion, causing stress concentrations during sliding in which ledges of opposites signs lock, giving as a result a viscoelastic response of the material. Without sliding to load multigrain junctions, cavitation will not occur, and it may cause creep rate decrease. The unelastic recovery observed in some crept ceramic materials may be the unloading of strained, but uncavitated multigrain junctions.

Diffusional creep prevails as sliding accommodation for composition A, for all temperatures and stresses used in this work. The stress exponent near unity indicates in these cases local stresses acting as driving forces for the solution-reprecipitation mechanisms, controlled either by rate of reactions of solution-reprecipitation at the interface crystalline/glassy phase or by rate of transport through intergranular phase. Cavities, mainly wedge-shaped, prevails for materials with higher anticipated glassy phase (B), under creep tests at and above 1350 °C (Fig. 14). These discontinuities can be originated from pre-existing defects from the sintering process, or vapor bubbles which grows inside the glass during creep test, as can be seen at Fig. 15, where such bubbles appears involving a grain of $Nd_2Si_3O_3N_4$ (N-melilite).

When diffusion does not prevail, viscous movement controlled by sliding rate of grain boundary can lead to elastic stress concentration at triple point junctions. The amount (extension) of sliding will be dependent upon volume and viscosity of the glassy phase at these regions. The growth of cavities in this situation would cause stress relaxation at triple point, allowing grain boundary sliding continuity. There is a progressive strain with subsequent cavity growth and new sliding.

The high number of wedge-cavities observed after creep test, at the composition with higher amount of glassy phase could be related to the higher probability of cavitation at thicker secondary glass phases at triple points. This higher probability is related to the higher surface energy for fracture originated from local compositional fluctuations [28]. At higher sliding

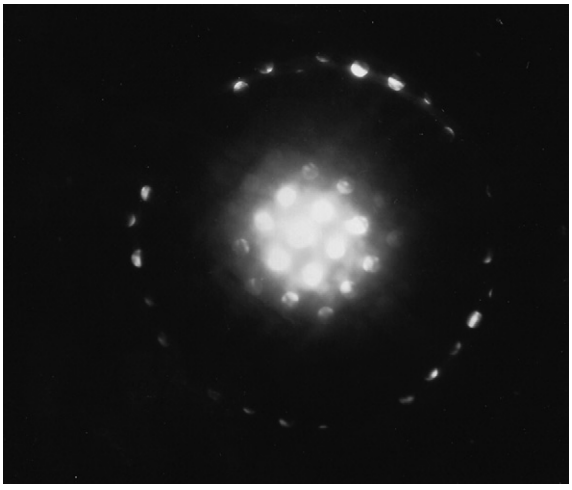

Fig. 13. X-ray diffraction pattern of N-melilite phases.

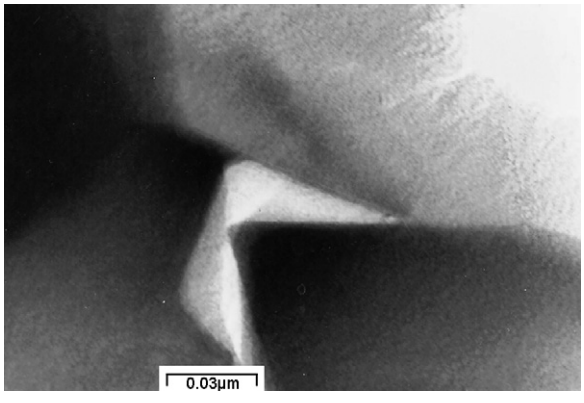

Fig. 14. Wedge cracks on crept samples of composition B.

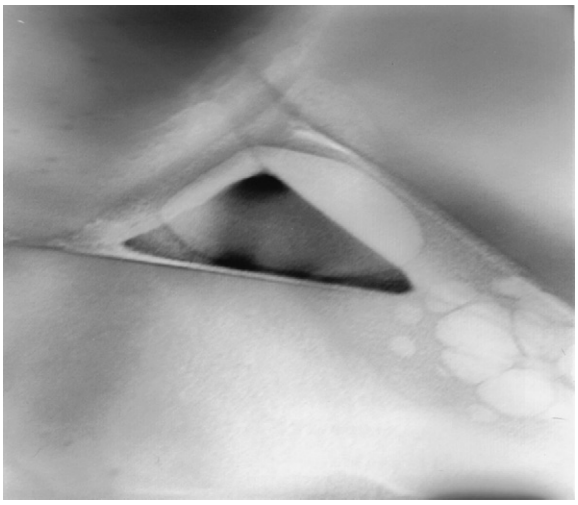

Fig. 15. Vapor bubbles at glass phase at grain junctions.

extension, prevalent for compositions with higher volume of intergranular glassy phase (B), the sliding overcomes the initial hydrostatic compression at silicate pockets. Cavities will form with subsequent flow of silicate, causing matter redistribution to surrounding pockets and, as a result, volume expansion. Grain boundary sliding will occurs to accommodate such expansion, causing loading at new multigrain pocket and cavitation creep. If load and temperature test conditions are high and amount and crystalline degree of intergranular phase are low in such a way that the accommodation process is not efficient, the growth of the cavities will proceed jacking the grains apart.

4. Conclusions

Under the creep testing conditions applied in this work, single thermally activated mechanism would prevail at each stress level during compressive strain at elevated temperatures, at silicon nitride based ceramic materials with low (8% neodymium oxide) and higher (8% yttrium/neodymium oxide) percentage of intergranular glass phase.

Diffusional creep with sliding accommodation by diffusion of ionic species is predominant at lower temperatures and lower stresses of creep tests, lower amount and higher crystalline degree of multigrain junctions and intergranular phases. The stress exponent near unity indicates in these cases local stress acting as driving forces for the solution-reprecipitation mechanisms, controlled either by rate of reactions of solution-reprecipitation at the interface crystalline/glassy phase or by rate of transport trough intergranular phase.

Wedge cavities, discernible by TEM, became prevalent with increase in amount and reduction of crystalline degree of the existing phase at grain boundary and multigrain junctions, for higher temperatures and stresses.

Cavities in fluids are dependent upon viscosity at the early stages [28]. It is considered that the initial growth of wedge cracks at the associated model with the present work is initially restricted (constricted) by the grain boundary sliding.

The cavitational creep at silicon nitride based compositions would be in this case, favored in situations where intergranular phase has greater thickness and lower viscosity.

References

[1] Q. Jin, D.S. Wilkinson, G.C. Weatherly, J. Am. Ceram. Soc. 79 (1996) 211–214.
[2] F. Ralph, J. Krause, J. Sheldon, Chien-Wei. Li, J. Am. Ceram. Soc. 10 (2001) 2394–2400.
[3] K.M. Fox, J.R. Hellmann, E.C. Dickey, D.J. Green, D.L. Shellemn, Z.R.L. Yeckley, J. Am. Ceram. Soc. 89 (2006) 2555–2563.
[4] M.A. Boling-Risser, K.C. Goretta, J.L. Routbort, K.T. Faber, J. Am. Ceram. Soc. 83 (2000) 3065–3069.
[5] P. Saigalik, J. Dusza, M.J. Hofman, J. Am. Ceram. Soc. 78 (10) (1995) 2619–2624.
[6] A. Rendtel, H. Hubner, M. Herrmann, C. Schubert, J. Am. Ceram. Soc. 81 (1998) 1109–1129.
[7] A. Rendtel, H. Hubner, M. Herrmann, C. Schubert, J. Am. Ceram. Soc. 81 (1998) 1095–1108.
[8] J. Crampon, R. Duclos, F. Peni, S. Guicciardi, G. De Portu, J. Am. Ceram. Soc. 80 (1) (1997) 85–91.
[9] S. Zhu, M. Mizuno, Y. Kagawa, J. Mater. Sci. 34 (1999) 1799–1807.
[10] M.K. Cinibulk, G. Thomas, S.M. Johnson, J. Am. Ceram. Soc. 75 (8) (1992) 2037–2043.
[11] M.K. Kerber, M.G. Genkins, J. Am. Ceram. Soc. 75 (9) (1992) 2543–2562.
[12] M.K. Kerber, M.G. Genkins, T.A. Nolan, R.L. Yeckley, J. Am. Ceram. Soc. 779 (3) (1994) 657–665.
[13] L.E. William, J. Am. Ceram. Soc. 85 (2002) 408–414.
[14] B.J. Hockley, S.M. Widerhorn, W. Liu, J.G. Baldoni, S.T. Buljan, J. Mater. Sci. 26 (1991) 3931–3939.
[15] W. Luecke, S.M. Widerhorn, B.J. Hocley, G.G. Long, Silicon Nitride Ceramics: Scientific and Technological Advances, in: I.-W. Chen, P.F. Becher, M. Mitomo, G. Petzow, T.S. Yen (Eds.), Materials Research Society Symposium Proceedings, Materials Research Society, Pittsburgh, PA, 287 (1993) 467–472.
[16] T. Ohji, Y. Yamauchi, S. Kanzaki, in: M. Hoffmann, G. Petzow, P.F. Becher (Eds.), Silicon Nitride, Trnas tech Aedermannsdorf, Switzerland, 1993, p. 92.
[17] C.J. Gasdaska, J. Am. Ceram. Soc. 77 (1994) 208–218.
[18] D.S. Wilkinson, J. Am. Ceram. Soc. 81 (2) (1998) 275–299.
[19] W.E. Ueke, S.M. Wiederhorn, B.J. Hockey, R.F. Krause, G.G. Long, J. Am. Ceram. Soc. 78 (8) (1995) 2085–2096.
[20] Julin Wan, Ren-Guan-Duan, J.G. Matthew, A.K. Mukherjee, J. Am. Ceram. Soc. 89 (2005) 274–280.
[21] M.K. Ferber, M.G. Jenkins, V.J. Tennery, Ceram. Eng. Sci. Proc. 11 (7) (1990) 1028–1045.
[22] W. Luecke, S.M. Wiederhorn, in: M. Hoffmann, G. Petzow, P.F. Becher (Eds.), Silicon Nitride '93, Trnas. Tech Aedermannsdorf, Switzerland, 1993, pp. 587–591.
[23] R. Raj, P.E.D. Morgan, J. Am. Ceram. Soc. 63 (1981), C-143–C-145.
[24] W. Braue, R.W. Carpenter, D.J. Smith, J. Mater. Sci. 25 (1990) 2949–2957.
[25] L.K.L. Falk, C.G. Dunlop, J. Mater. Sci. 22 (1987) 4369–4376.
[26] F.F. Lange, B.I. Davis, D.R. Clarke, J. Mater. Sci. 15 (1980) 601–610.
[27] R. Raj, C.K. Chyung, Acta Metall. 29 (1981) 159–166.
[28] D.R. Clarke, in: M.J. Hofmann (Ed.), Taloring of Mechanical Properties of Si_3N_4 Ceramics, Kluwer, Dordrecht, The Netherlands, 1994, pp. 291–301.
[29] W.R. Cannon, G.T. Langdon, J. Mater. Sci. 18 (1983) 1–50.